Active glassy dynamics is unaffected by the microscopic details of self-propulsion

Please check the document version of this publication:

• A submitted manuscript is the version of the article upon submission and before peer-review. There can be important differences between the submitted version and the official published version of record. People interested in the research are advised to contact the author for the final version of the publication, or visit the DOI to the publisher's website.
• The final author version and the galley proof are versions of the publication after peer review.
• The final published version features the final layout of the paper including the volume, issue and page numbers.

Link to publication

Active glassy dynamics is unaffected by the microscopic details of self-propulsion

Vincent E. Debets and Liesbeth M. C. Janssen

View Online   Export Citation   CrossMark

ARTICLES YOU MAY BE INTERESTED IN

AIP Publishing

Active glassy dynamics is unaffected by the microscopic details of self-propulsion

Vincent E. Debets[1,2] (iD) and Liesbeth M. C. Janssen[1,2,a] (iD)

AFFILIATIONS

[1] Department of Applied Physics, Eindhoven University of Technology, P.O. Box 513, 5600 MB Eindhoven, The Netherlands
[2] Institute for Complex Molecular Systems, Eindhoven University of Technology, P.O. Box 513, 5600 MB Eindhoven, The Netherlands

[a] Author to whom correspondence should be addressed: l.m.c.janssen@tue.nl

ABSTRACT

Recent years have seen a rapid increase of interest in dense active materials, which, in the disordered state, share striking similarities with the conventional passive glass-forming matter. For such passive glassy materials, it is well established (at least in three dimensions) that the details of the microscopic dynamics, e.g., Newtonian or Brownian, do not influence the long-time glassy behavior. Here, we investigate whether this still holds true in the non-equilibrium active case by considering two simple and widely used active particle models, i.e., active Ornstein-Uhlenbeck particles (AOUPs) and active Brownian particles (ABPs). In particular, we seek to gain more insight into the role of the self-propulsion mechanism on the glassy dynamics by deriving a mode-coupling theory (MCT) for thermal AOUPs, which can be directly compared to a recently developed MCT for ABPs. Both theories explicitly take into account the active degrees of freedom. We solve the AOUP- and ABP-MCT equations in two dimensions and demonstrate that both models give almost identical results for the intermediate scattering function over a large variety of control parameters (packing fractions, active speeds, and persistence times). We also confirm this theoretical equivalence between the different self-propulsion mechanisms numerically via simulations of a polydisperse mixture of active quasi-hard spheres, thereby establishing that, at least for these model systems, the microscopic details of self-propulsion do not alter the active glassy behavior.

Published under an exclusive license by AIP Publishing. https://doi.org/10.1063/5.0127569

INTRODUCTION

The study of active matter has been gaining widespread attention in the field of colloidal and biological physics since the beginning of the previous decade.[1–3] While much focus has already been dedicated to dilute and moderately dense self-propelled particle suspensions, recent years have also seen a rising interest in high-density active materials.[4,5] Interestingly, when self-propelled particles are pushed to sufficiently high densities, regardless of their intrinsic driving, they will manifestly become kinetically arrested and, in fact, show a strong resemblance to more conventional passive glassy materials. This so-called active glassy behavior has indeed been reported in the context of, e.g., living cells[6–12] and colloidal and granular experiments,[13–15] while it has also been observed in multiple theoretical and simulation studies.[16–38] Intuitively, it might be expected that dense active matter will eventually be dominated by interactions. However, activity can certainly influence glassy materials in non-trivial ways.[18,21,22,24–26,36,38] The question of what this influence precisely encompasses and to what degree it depends on the specific details of the active self-propulsion mechanism, has, therefore, unfolded itself as an increasingly interesting new area of research.

Two of the simplest and most widely studied models in (dense) active matter are so-called active Brownian particles (ABPs) and active Ornstein Uhlenbeck particles (AOUPs). Their difference rests in the implementation of the self-propulsion force, which either has a constant magnitude and undergoes rotational diffusion (ABPs) or evolves in time according to an Ornstein-Uhlenbeck process (AOUPs). This difference, however, is washed out on a coarse-grained level where the active degrees of freedom are integrated out, in which case both models become identical.[20] Since most theoretical attempts to study dense assemblies of these model active particles have required coarse-graining,[17–20,39,40] it has not yet

been possible to pinpoint the effect of the specific self-propulsion mechanism on the glassy dynamics.

An exception to the coarse-grained strategy is recent work where a mode-coupling theory (MCT) for ABPs has been developed in which the active degrees of freedom, i.e., the orientations of the active force, are explicitly taken into account.[16,28–30] This has revealed several non-trivial short-time features that cannot be captured when employing coarse-grained approaches. A key question, however, remains whether these microscopic details play a significant role in the long-time glassy dynamics of dense active matter. For passive systems, it is well-confirmed that (at least in three-dimensional systems) both Brownian and Newtonian dynamics yield identical long-time behavior, and hence, the microscopic details of motion are irrelevant for the glassy dynamics. This has been demonstrated both in theory and simulations.[41–45] It would be interesting to see if such an equivalence is maintained for active systems. Since particle motion becomes more impeded by repulsion at high densities, one would expect the precise single-particle dynamics, whether active or passive, to become increasingly less relevant.

Here, we shed more light on the influence of the self-propulsion mechanism on active glassy dynamics from a theoretical perspective. We provide, for the first time, a detailed derivation of a mode-coupling theory for thermal AOUPs that explicitly takes into account the active degrees of freedom. Our theory, which is based on similar principles as the recently developed MCT for ABPs,[16,28–30] thus allows for a convenient comparison between both models in the high-density regime. We numerically solve the relevant equations and show that for a wide variety of different settings (packing fractions, active speeds, and persistence times) ABPs and AOUPs give almost identical results after mapping their single-particle dynamics onto each other. To further verify the equivalence between both active self-propulsion models, we also directly compare our theoretical results to ones obtained from simulations of a polydisperse mixture of self-propelled quasi-hard spheres.

THEORY

Active particle models

Both the ABP and AOUP model describe a two-dimensional (2D) N-particle active fluid of area V (and number density $\rho = N/V$) as a collection of self-propelling and interacting particles. In particular, each particle i within the fluid evolves in time t according to Refs. 1, 20, 22, and 39,

$$\frac{d\mathbf{r}_i}{dt} = \zeta^{-1}(\mathbf{F}_i + \mathbf{f}_i) + \boldsymbol{\xi}_i. \tag{1}$$

Here, $\mathbf{r}_i$ denotes the position of particle i, ζ the friction constant, $\mathbf{F}_i$ and $\mathbf{f}_i$ the interaction and self-propulsion force acting on particle i, respectively, and $\boldsymbol{\xi}_i$ a Gaussian thermal noise with zero mean and variance $\left\langle \boldsymbol{\xi}_i(t)\boldsymbol{\xi}_j(t') \right\rangle_{\text{noise}} = 2D\mathbf{I}\delta_{ij}\delta(t-t')$, with D the thermal diffusion coefficient and $\mathbf{I}$ the unit matrix. The distinction between both models resides in the dynamics of the self-propulsion force $\mathbf{f}_i$. For AOUPs, the time evolution of the self-propulsion force is governed by an Ornstein-Uhlenbeck process,[18–20,23,25,26]

$$\frac{d\mathbf{f}_i}{dt} = -\tau^{-1}\mathbf{f}_i + \boldsymbol{\eta}_i, \tag{2}$$

where τ depicts the typical decay time of the self-propulsion and $\boldsymbol{\eta}_i$ an internal Gaussian noise process with zero mean and a variance $\left\langle \boldsymbol{\eta}_i(t)\boldsymbol{\eta}_j(t') \right\rangle_{\text{noise}} = 2D_f\mathbf{I}\delta_{ij}\delta(t-t')$ whose amplitude is controlled by the noise strength D_f. In contrast, the ABP model assumes a constant absolute value of the self-propulsion speed v_0, so that $\zeta^{-1}\mathbf{f}_i = v_0\mathbf{e}_i = v_0[\cos(\theta_i), \sin(\theta_i)]$, and lets the orientation angles θ_i undergo rotational diffusion with a diffusion coefficient D_r. This yields[1,16,17]

$$\dot{\theta}_i = \chi_i, \tag{3}$$

with χ_i a Gaussian noise process with zero mean and variance $\left\langle \chi_i(t)\chi_j(t') \right\rangle_{\text{noise}} = 2D_r\delta_{ij}\delta(t-t')$.

Without particle–particle interactions, both models predict a persistent random walk (PRW), which implies that the mean square displacement (MSD) of each particle is given by[20]

$$\left\langle \delta r^2(t) \right\rangle = 4Dt + 2v_a^2\tau_p\left(\tau_p(e^{-t/\tau_p} - 1) + t\right). \tag{4}$$

The parameters describing such a PRW are the persistence time, $\tau_p = \tau$ (AOUP), $\tau_p = (D_r)^{-1}$ (ABP), an (average) active speed $v_a = v_0$ (ABP), $v_a = \sqrt{2D_f\tau_p}\zeta^{-1}$ (AOUP), and the thermal diffusion coefficient D. On the single-particle level, both models can thus strictly be mapped onto each other via the equivalency of their MSDs.

Mode-coupling theory

To infer information on the collective level, we require the joint N-particle probability distribution of positions and self-propulsion forces/orientation angles $P_N(\Gamma; t)$. This distribution is governed by the equation,

$$\frac{\partial}{\partial t}P_N(\Gamma; t) = \Omega P_N(\Gamma; t), \tag{5}$$

with $\Gamma = (\Gamma_T, \Gamma_R) = (\mathbf{r}_1, \ldots, \mathbf{r}_N, \mathbf{f}_1, \ldots, \mathbf{f}_N)$ (AOUP), $\Gamma = (\Gamma_T, \Gamma_R) = (\mathbf{r}_1, \ldots, \mathbf{r}_N, \theta_1, \ldots, \theta_N)$ (ABP) denoting the configuration space, and Ω the evolution operator (see Refs. 16 and 19 for detailed definitions of the latter). Now, we assume that our systems can reach a steady-state characterized by a probability distribution $P_N^{ss}(\Gamma)$ that obeys[17,19]

$$\Omega P_N^{ss}(\Gamma) = 0. \tag{6}$$

In principle, we can then study our systems by calculating steady-state averages via

$$\left\langle \ldots \right\rangle = \int d\Gamma \ldots P_N^{ss}(\Gamma). \tag{7}$$

However, the steady-state distribution is typically not known exactly. To proceed and make calculations tractable, we will, therefore, approximate our steady-state averages according to

$$\langle \ldots \rangle \approx \int d\Gamma \ldots P_{\text{eq}}(\Gamma_{\text{T}}) P(\Gamma_{\text{R}}), \tag{8}$$

where, for the AOUP model,

$$P(\Gamma_{\text{R}}) = \frac{1}{(2\pi D_f \tau_p)^{dN/2}} \exp\left(-\frac{\sum_i \mathbf{f}_i^2}{2 D_f \tau_p}\right)$$

$$= \prod_{i=1}^{N} \frac{1}{(2\pi D_f \tau_p)^{d/2}} \exp\left(-\frac{\mathbf{f}_i^2}{2 D_f \tau_p}\right) \equiv \prod_{i=1}^{N} p(\mathbf{f}_i), \tag{9}$$

represents the distribution of self-propulsion forces, which is factorized in independent Gaussian single-particle distributions $p(\mathbf{f}_i)$, while for the ABP model it is simply $P(\Gamma_{\text{R}}) = (2\pi)^{-N}$. Note that $d = 2$ depicts the dimensionality of the system. The distribution of particle positions is the same for both models and given by the Boltzmann solution, $P_{\text{eq}}(\Gamma_{\text{T}}) \propto \exp(-\beta U(\Gamma_{\text{T}}))$. This distribution depends solely on the total interaction potential $U(\Gamma_{\text{T}})$, which induces the interaction forces $\mathbf{F}_i = -\nabla_i U(\Gamma_{\text{T}})$. Moreover, we assume throughout that the Stokes-Einstein equation connects the inverse thermal energy β to the friction constant via $\beta D = \zeta$. As a first approximation, we thus calculate averages based on the distribution the system would assume if the influence of the active forces becomes negligibly small; it, therefore, neglects any correlations between particle velocities and positions[10,26,46] (though we have checked in simulations that these remain relatively small due to the presence of thermal noise) and becomes exact in the limit $v_a \to 0$. Note that, in principle, this approximation is similar to the lowest order one in the integration-through-transients formalism, which has been employed in previous work on mode-coupling theory for ABPs and colloidal suspensions under shear flow.[16,28–30,47] In this formalism, one typically uses transient correlation functions defined with the equilibrium average to find exact expressions for transport coefficients. It has, for instance, been used to calculate macroscopic stresses in colloidal suspensions.

In standard mode-coupling theory, the starting point to study the glassy dynamics of a system is the set of density modes.[48–50] Since we want to explicitly include active degrees of freedom, these become more complex in active-MCT and are given by[51]

$$\rho_l(\mathbf{k}) = \begin{cases} \dfrac{i^{m+n}}{\sqrt{N}} \sum_{j=1}^{N} e^{i\mathbf{k}\cdot\mathbf{r}_j} H_m(\bar{f}_{j,x}) H_n(\bar{f}_{j,y}), & \text{(AOUP)} \\[2ex] \dfrac{1}{\sqrt{N}} \sum_{j=1}^{N} e^{i\mathbf{k}\cdot\mathbf{r}_j} e^{il\theta_j}, & \text{(ABP)} \end{cases} \tag{10}$$

Here, $H_m(x)$ denotes a normalized Hermite polynomial [see Eq. (A3)] and $\bar{\mathbf{f}} \equiv \mathbf{f}/\sqrt{2 D_f \tau_p}$ a dimensionless self-propulsion force. For compactness of notation, we have introduced the index l as a general label for both AOUPs and ABPs; for AOUPs it corresponds to the degree of the Hermite polynomials $l = \{m, n\}$ with $m, n \in [0, \infty]$, whereas for ABPs it corresponds to the angular mode $l \in [-\infty, \infty]$. The equilibrium-averaged (also called transient) time-correlation between such density modes can then be defined via

$$S_{l;l'}(\mathbf{k}, t) = \left\langle \rho_l^*(\mathbf{k}) e^{\Omega^\dagger t} \rho_{l'}(\mathbf{k}) \right\rangle, \tag{11}$$

with $\Omega^\dagger$ the adjoint evolution operator [see Eq. (A6) and Ref. 16], which works on everything to its right except for the probability distribution. Note that the lowest order term $S_{0;0}(\mathbf{k}, t) \equiv F(k, t)$ is the same for both models and corresponds to the (transient) intermediate scattering function. It will, therefore, serve as the main probe to study the glassy dynamics of our active systems. Moreover, at time zero, assuming our systems to be isotropic, the density correlation functions are easily calculated and yield

$$S_{l;l'}(k) = \left\langle \rho_l^*(\mathbf{k}) \rho_{l'}(\mathbf{k}) \right\rangle = \delta_{ll'}[1 + \delta_{l0}(S(k) - 1)], \tag{12}$$

where $S(k)$ denotes the equilibrium static structure factor, which, for instance, can be obtained from liquid state theory or simulations.

We now follow the mode-coupling strategy pioneered for ABPs in Ref. 16 and apply it to AOUPs. The full AOUP MCT derivation is detailed in Appendix A. We finally arrive at the following general equation of motion for the dynamic density correlation functions of both models,

$$\frac{\partial}{\partial t} S_{l;l'}(\mathbf{k}, t) + \sum_{l_1} \omega_{l;l_1}(\mathbf{k}) S_{l_1;l_1}^{-1}(k) S_{l_1;l'}(\mathbf{k}, t)$$

$$+ \int_0^t dt' \sum_{l_1 l_2} M_{l;l_1}(\mathbf{k}, t - t') [\omega_{l_1;l_2}^{\text{T}}(\mathbf{k})]^{-1}$$

$$\times \left[\frac{\partial}{\partial t'} S_{l_2;l'}(\mathbf{k}, t') + \omega_{l_2;l_2}^{\text{R}} S_{l_2;l'}(\mathbf{k}, t') \right] = 0, \tag{13}$$

where $\omega_{l;l'}(\mathbf{k})$ represents the collective diffusion tensor, which governs the short-time dynamics and is split in a translational (T) and rotational (R) term. The memory kernel encodes all non-trivial dynamics and is given by

$$M_{l;l'}(\mathbf{k}, t) \approx \frac{\rho}{2} \int \frac{d\mathbf{q}}{(2\pi)^2} \sum_{l_1 l_2} \sum_{l_3 l_4} V_{l l_1 l_2}(\mathbf{k}, \mathbf{q}, \mathbf{k} - \mathbf{q})$$

$$\times S_{l_1;l_3}(\mathbf{q}, t) S_{l_2;l_4}(\mathbf{k} - \mathbf{q}, t) V_{l' l_3 l_4}^{\text{eq}}(\mathbf{k}, \mathbf{q}, \mathbf{k} - \mathbf{q}), \tag{14}$$

For specific details of the involved parameters, in particular, the vertices $V_{l l_1 l_2}(\mathbf{k}, \mathbf{q}, \mathbf{k} - \mathbf{q})$ and $V_{l l_1 l_2}^{\text{eq}}(\mathbf{k}, \mathbf{q}, \mathbf{k} - \mathbf{q})$, and a precise derivation we refer to Ref. 16 and Appendix A. We mention that in comparison to the more familiar passive MCT equation,[52] the equation of motion now includes a so-called hopping term $\omega_{l_2;l_2}^{\text{R}} S_{l_2;l'}(\mathbf{k}, t')$ inside the time integral. This term ensures the long-time decay of the active degrees of freedom.[16] Importantly, it must be emphasized that, although the structure of the MCT equation of motion is similar for both models, the individual terms in the equation are not necessarily the same. Most notably the collective diffusion tensor $\omega_{l;l'}(\mathbf{k})$ and the left vertex $V_{l l_1 l_2}(\mathbf{k}, \mathbf{q}, \mathbf{k} - \mathbf{q})$ harbor the key differences between the AOUP and ABP model.

To summarize, using only the equilibrium static structure factor $S(k)$, the persistence time τ_{p}, active speed v_a, and area fraction ϕ (or number density ρ) as input parameters, we can self-consistently find a solution for $S_{l;l'}(\mathbf{k}, t)$ and, in particular, for the intermediate scattering function $F(k, t)$. The latter can then be used to compare the glassy behavior of both models in the high-density regime.

METHODS

Active-MCT numerics

To establish proof of principle, we numerically solve the active-MCT equations for a monodisperse colloidal mixture of hard disks of diameter σ. For such a mixture one can employ an analytical expression for $S(k)$ (as a function of the area fraction $\phi = \rho\pi\sigma^2$) based on density functional theory.[53] The two-dimensional integral over $\mathbf{q}$ in the memory kernel [Eq. (14)] is rewritten in terms of the coordinates $q = |\mathbf{q}|$ and $p = |\mathbf{k} - \mathbf{q}|$, whose individual integrals are performed on an equidistant wavenumber grid $k\sigma = [0.6, 1.0, \ldots, 39.8]$. Note that we drop the smallest wavenumber $k\sigma = 0.2$ in favor of numerical stability. For computational convenience, we only take into account the lowest order non-trivial active modes, i.e., $l \in [\{0, 0\}, \{1, 0\}, \{0, 1\}]$ (AOUP) and $l \in [-1, 0, 1]$ (ABP). It is important to realize that taking the inverse of $\omega_{ll'}^{\mathrm{T}}(\mathbf{k})$, in principle, does not commute with the cutoff f active modes. We have checked that taking the inverse at a larger cutoff (up to 20 non-trivial active modes) and afterward reducing to the lowest order active modes induces slight quantitative changes but does not qualitatively change our results. Overall, the used cutoff yields stable solutions for the presented range of active speeds and persistence times, although we mention that above the idealized glass transition, instabilities on very long time scales still persist. To handle the fact that higher order correlation functions ($S_{l;l'}(\mathbf{k}, t)$ with $l, l' \neq \{0, 0\}, 0$) depend explicitly on the orientation of the wavevector $\mathbf{k}$, we can invoke transformation rules that enable us to rewrite correlators with wavevector $\mathbf{k}$ in terms of ones with a rotated wavevector $\mathbf{k}'$ (see Ref. 16 and Appendix B for precise details). We can, therefore, restrict our discussion to wavevectors aligned along a specific direction, which we have chosen to be the x-axis, i.e., $\mathbf{k} = k\mathbf{e}_x$. Finally, we fix the passive diffusion coefficient at $D = 1$ so that our unit of time equals σ^2/D and perform the integration over time in Eq. (13) according to the algorithm presented in Ref. 16. For this, we calculate the first $N_t/2 = 16$ points in time using a Taylor expansion with a step size $\Delta t = 10^{-6}$, numerically integrate the equations of motion for the next $N_t/2$ points in time, duplicate the timestep, and repeat the process.

Simulation details

To complement our theoretical results, we also simulated both the AOUP and ABP dynamics of a slightly polydisperse mixture of $N = 1000$ quasi-hard disks. Each particle i is described by Eq. (1) and the interaction force $\mathbf{F}_i = -\sum_{j \neq i} \nabla_i V_{\alpha\beta}(r_{ij})$ is derived from a quasi-hard-sphere powerlaw potential $V_{\alpha\beta}(r) = \epsilon\left(\frac{\sigma_{\alpha\beta}}{r}\right)^{36}$.[54,55] The interaction energy ϵ, friction constant ζ, and diffusion coefficient D are all set to a value of one. To ensure polydispersity, our mixture consists of equal fractions of particles with diameters (in units of σ) $\sigma_{\alpha\alpha} = \{0.8495, 0.9511, 1.0, 1.0489, 1.1505\}$,[56] which are additive so that $\sigma_{\alpha\beta} = (\sigma_{\alpha\alpha} + \sigma_{\beta\beta})/2$. Simulations are performed by solving the Langevin equation [Eq. (1)] via a forward Euler scheme and are carried out using Large-scale Atomic/Molecular Massively Parallel Simulator (LAMMPS).[57] We fix the square box size to set the area fraction at $\phi = 0.75$ (higher values tend to result in crystallization) and impose periodic boundary conditions. We then set the persistence time τ_p and active speed v_a, run the system

sufficiently long to ensure no aging takes place, and afterward track the particles over time. All simulation results are presented in units where σ, ϵ, and $\zeta\sigma^2/\epsilon$ denote the units of length, energy, and time, respectively.[42]

RESULTS AND DISCUSSION

Before proceeding to the glassy dynamics, we first briefly discuss the free-particle dynamics in more detail to elucidate potential intrinsic differences between both models. For this, we exploit the fact that at zero density the memory kernel can be set to zero and that $S(k) = 1$.[16] This allows us to exactly solve Eq. (13), which yields $\mathbf{S}(\mathbf{k}, t) = \exp(-\boldsymbol{\omega}(\mathbf{k})t)$. Based on this result, we have calculated the intermediate scattering function $F(k, t)$ for different active speeds and persistence times and have plotted the results in Fig. 1. Note that the free-particle solution allows for the inclusion of many active modes, and we have verified that these results remain unaltered upon adding more active modes. An inspection of Fig. 1 shows that $F(k, t)$ decays more rapidly upon increasing the active speed or persistence time. Moreover, at a large wavenumber $k = 6.6$ both models give the same results, which is consistent with our initial mapping of the single-particle MSDs [see Eq. (4)]. Interestingly, it can be seen that at a relatively small wavenumber, $k = 1.0$, differences between both models start to manifest themselves, especially at larger values of the active speed and persistence time. In particular, the ABP model yields oscillatory behavior, which has been attributed to the persistent swimming of the ABPs.[58,59] These oscillations are absent

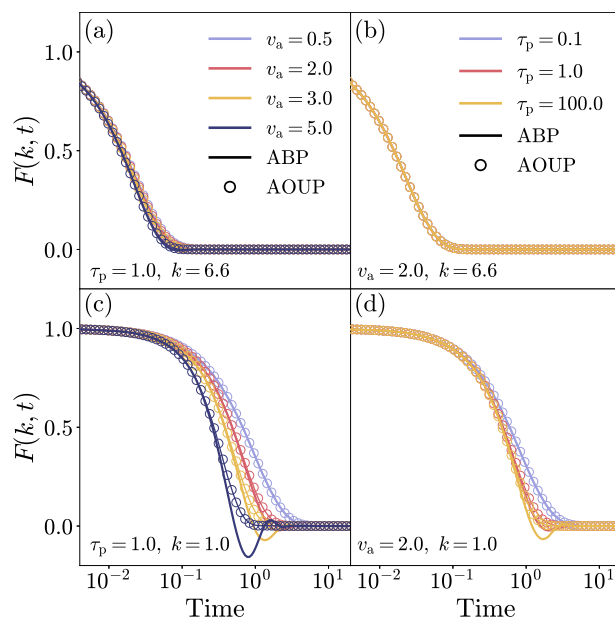**FIG. 1.** The intermediate scattering function $F(k, t)$ for free particles ($\rho = 0$) as a function of time obtained for both ABP-MCT (solid lines) and AOUP-MCT (circles) at (a) and (b) a wavevector $k = 6.6$ close to the first peak of the static structure factor and (c) and (d) a relatively small wavevector $k = 1.0$. Results correspond to (a) and (c) different active speeds, and (b) and (d) different persistence times.

for the AOUPs since the Ornstein-Uhlenbeck process is Gaussian and correlation functions, therefore, should decay monotonically. A mapping based on the MSD, which is essentially a zero-wavenumber limit of the density correlation function, thus misses these differences at finite k. In other words, the free-particle intermediate scattering function $F(k,t)$ ($\rho = 0$) can distinguish between the ABP and AOUP models.

Let us now look at the theoretical predictions of the ABP- and AOUP-MCT frameworks at high densities to understand their glassy behavior and see whether the single-particle differences between both models persist in the glassy regime. To compare both models, we have primarily focused on the intermediate scattering function $F(k,t)$, which has been plotted for a variety of different settings and both models in Fig. 2. We note that, despite the presence of an active self-propulsion mechanism, both ABP-MCT and AOUP-MCT still predict an idealized glass transition upon increasing the packing fraction (or density). This is characterized by the emergence of a nonzero long-time value for $F(k,t)$. Moreover, we see that increasing the active speed v_a and the persistence time τ_p always yields faster relaxation dynamics, represented by a more rapid decay to zero of $F(k,t)$. These predictions are all consistent with the previous in-depth study of ABP-MCT and simulations of a polydisperse mixture of self-propelling hard spheres,[16,22] though we mention that an increase of the persistence time at a fixed effective temperature (instead of the active speed) can also yield non-monotonic behavior.[18] This reentrant dynamics has already been qualitatively predicted by a recently developed MCT for athermal AOUPs[18,19] and rationalized in terms of efficient cage exploration.[36]

More strikingly, however, we observe that for all shown cases and all considered time scales, both models predict almost identical results. This implies that, at least in the numerically accessible region, the mapping between ABPs and AOUPs based on the single-particle MSDs [Eq. (4)] transfers directly to the collective structural relaxation in the high-density regime. Interestingly, for a relatively small wavenumber $k = 1.0$ the differences on the single-particle level [see Figs. 1(c) and 1(d)] have even been washed out in the glassy regime with $F(k,t)$ in all cases decaying monotonically. Since an oscillatory decay of $F(k,t)$ has been attributed to persistent swimming of the ABPs, we expect that this is suppressed by particle–particle interactions at high densities. This in turn forces the models to become more equivalent and give almost identical results. We have also verified that this equivalence occurs over an even larger parameter range than presented in Fig. 2. This suggests that, at least for the chosen model systems, the long-time dynamics does not depend on the microscopic details of the active self-propulsion, which is consistent with recent simulations of (a) thermal ABPs and AOUPs where a different parameter regime (larger active speeds and smaller persistence times) has been probed.[36] An important consequence of this equivalence might reside in the modeling of more complex dense active systems, such as confluent cell layers.[35,60] For such systems, it is often hard to infer precise details of the microscopic self-propulsion mechanism. Our results suggest that these details might be of lesser importance when studying high-density active matter.

To place our theoretical findings in a broader context, we now proceed to the predictions from our simulations. Based on
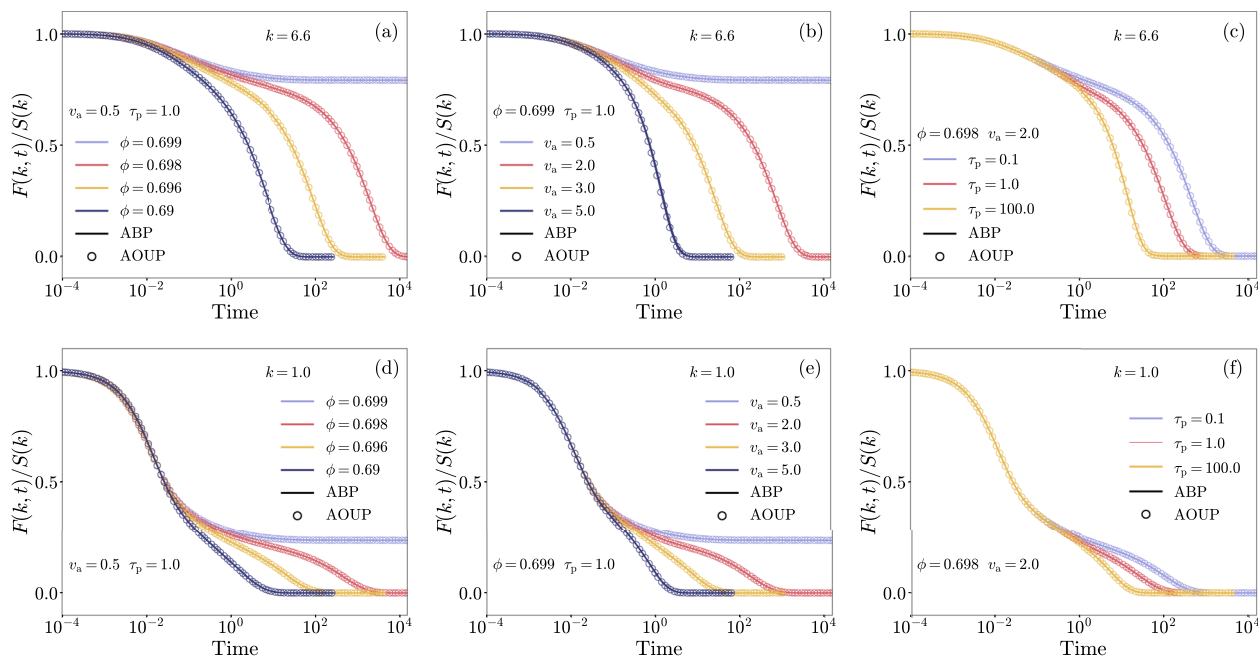
FIG. 2. The normalized intermediate scattering function $F(k,t)/S(k)$ as a function of time obtained for both ABP-MCT (solid lines) and AOUP-MCT (circles) at (a)–(c) a wavevector $k = 6.6$ close to the first peak of the static structure factor and (d)–(f) a relatively small wavevector $k = 1.0$. Results correspond to (a) and (d) different packing fractions, (b) and (e) different active speeds, and (c) and (f) different persistence times.
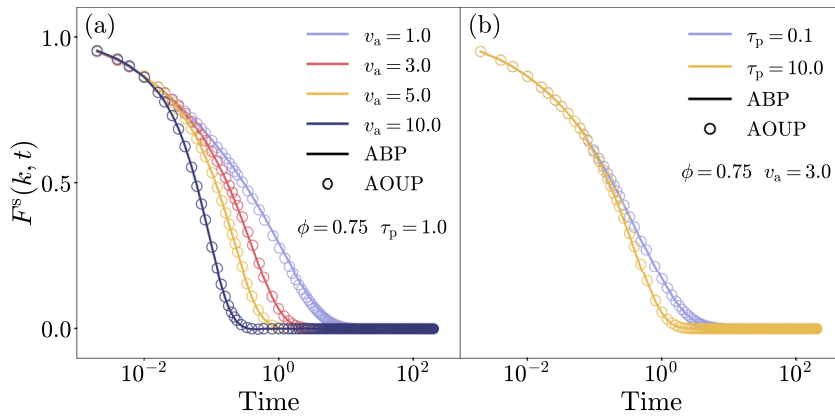
FIG. 3. The self-intermediate scattering function $F^s(k, t)$ as a function of time obtained from both ABP and AOUP simulations at a wavevector $k = 6.6$ close to the first peak of the static structure factor. Results correspond to different (a) active speeds, and (b) persistence times.
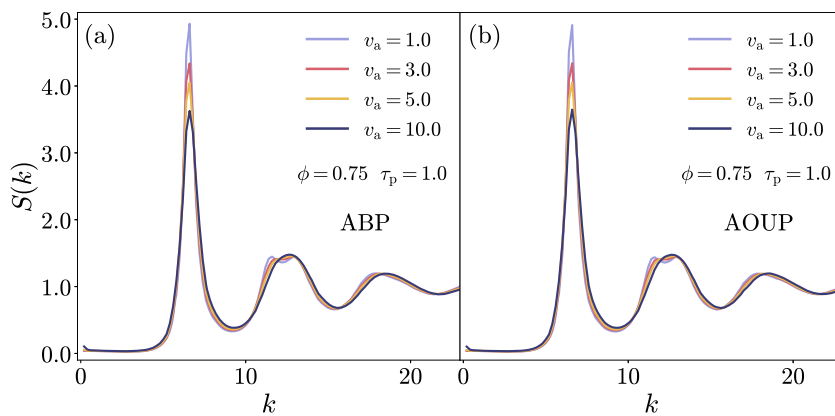

FIG. 4. The static structure factor $S(k)$ as a function of the wavevector k obtained from both (a) ABP and (b) AOUP simulations. Results correspond to different active speeds.

the retrieved particle trajectories, we have calculated the self-intermediate scattering function, i.e., $F^s(k, t) = \left\langle e^{-i\mathbf{k}\cdot\mathbf{r}_j(0)} e^{i\mathbf{k}\cdot\mathbf{r}_j(t)} \right\rangle$, where we mention that in simulations the statistical averaging is done with respect to the active steady-state. However, at high densities, the differences between steady-state and transient self-intermediate scattering functions have been found to be small (see Ref. 28 for a more detailed discussion). The results for both models are plotted for a variety of settings in Fig. 3. It can be seen that the relaxation of the self-intermediate scattering function occurs on shorter timescales upon increasing the active speed v_a [Fig. 3(a)] or the persistence time τ_p [Fig. 3(b)]. These results are qualitatively consistent with our theoretical predictions for the intermediate scattering function and imply that enhanced particle speed and persistence render the material more liquid-like.

Interestingly, we find that, also for our simulation results, the differences between both model systems are manifestly only marginal. This further substantiates our theoretical predictions and indicates that for simple model active systems the active glassy dynamics is unaffected by the microscopic details of active self-propulsion. This behavior is analogous to more conventional passive glass-forming materials, where it is well established that, at least in three dimensions, different single-particle dynamics, e.g., Newtonian or Brownian, yield similar long-time dynamics.[41–44]

We finalize our discussion by mentioning that a critical assumption in the presented active-MCT theories is the replacement of the steady-state probability distribution by its equilibrium counterpart. In other words, we assume the same (passive) structure for both models. Although unlikely, structural differences between both models might, therefore, still exist. To verify that our mapping of the dynamics also yields similar structures, we have retrieved the static structure factor, i.e., $S(k) = \left\langle \sum_{j=1}^{N} e^{-i\mathbf{k}\cdot\mathbf{r}_j} \sum_{l=1}^{N} e^{i\mathbf{k}\cdot\mathbf{r}_l} \right\rangle$, for the same parameters as for the self-intermediate scattering function. The results for different active speeds are plotted in Fig. 4. Consistent with the dynamical quantities we see that the static structure factor also remains almost unaltered when we interchange the ABP and AOUP models. Moreover, we see the height of the first peak decreasing upon increasing the active speed of the particles, which is consistent with the faster relaxation dynamics observed for the self-intermediate scattering function.

CONCLUSION

In this work, we have presented the first derivation of an MCT for thermal AOUPs that explicitly takes into account the active degrees of freedom (self-propulsion forces) via the density modes. Our derivation is based on previous work on ABP-MCT and uses the same assumption of replacing steady-state averages with their

equilibrium-averaged or transient counterparts. The central result comprises an equation of motion for the (transient) intermediate scattering function, which can be self-consistently solved using only the equilibrium static structure factor and relevant control parameters (packing fraction, active speed, and persistence time) as input.

Interestingly, after mapping both models on the single-particle (or non-interacting) level via their MSDs, our newly developed AOUP-MCT gives almost identical results as ABP-MCT over a wide range of values for the different control parameters. In other words, the equivalence of both models in the non-interacting regime transfers directly to the collective relaxation in the high-density (glassy) regime. Although this is consistent with recent simulation results,[36] we have further confirmed the witnessed equivalence between the different self-propulsion mechanisms by performing simulations of a polydisperse mixture of active quasi-hard spheres. In all cases, the differences between the AOUP and ABP simulations are minute. We thus conclude that, at least for the considered model systems, the microscopic details of the self-propulsion do not affect the active glassy behavior.

As a follow-up, it would be intriguing to see whether the witnessed equivalence between both models in the glassy regime can also be formally established given that the structure of the derived MCT equations is already identical. This could provide crucial theoretical insight into the emergent universality of dense active matter. A possible starting point for it might be to try to convert the Hermite-polynomial basis for the AOUPs into the trigonometric one adopted for the ABPs. Alternatively, one can look into the scaling laws close to the idealized glass transition, which have already been extensively studied for passive MCT.[49]

It could also be interesting to test the validity of the observed equivalence for more complex active self-propulsion models or when transitioning from overdamped to underdamped active dynamics (from microswimmers to so-called microflyers[61]). Finally, we mention that the derivation of AOUP-MCT can be easily extended to three dimensions. We, therefore, hope that the framework of AOUP-MCT will continue to be used for comparison with simulation or experimental results in order to better understand the rich phenomenology of active glassy matter.

AUTHOR DECLARATIONS

Conflict of Interest

The authors have no conflicts to disclose.

Author Contributions

Vincent E. Debets: Conceptualization (equal); Investigation (lead); Methodology (lead); Visualization (lead); Writing – original draft (lead); Writing – review & editing (equal). **Liesbeth M. C. Janssen**: Conceptualization (equal); Funding acquisition (lead); Resources (lead); Supervision (lead); Writing – review & editing (equal).

DATA AVAILABILITY

The data that support the findings of this study are available from the corresponding author upon reasonable request.

APPENDIX A: DERIVATION OF AOUP-MCT

As our starting point for the AOUP-MCT derivation, we take the following fluctuating local density to describe the collective motion of 2D AOUPs,

$$\rho(\mathbf{r}, \mathbf{f}) = \frac{1}{p(\mathbf{f})} \sum_{i=1}^{N} \delta(\mathbf{r} - \mathbf{r}_i)\delta(\mathbf{f} - \mathbf{f}_i)$$

$$= \pi^{3/2} \exp(\bar{\mathbf{f}}^2) \sum_{i=1}^{N} \delta(\mathbf{r} - \mathbf{r}_i)\delta(\bar{\mathbf{f}} - \bar{\mathbf{f}}_i). \quad (A1)$$

Here, we have introduced a dimensionless self-propulsion force $\bar{\mathbf{f}} \equiv \mathbf{f}/\sqrt{2D_f\tau_p}$ and added a prefactor for normalization. Next, we Fourier-Hermite expand the microscopic density, i.e.,

$$\rho(\mathbf{r}, \mathbf{f}) = \frac{1}{V} \sum_{\mathbf{k}} \sum_{mn} (-i)^{m+n} \rho_{mn}(\mathbf{k}) e^{-i\mathbf{k}\cdot\mathbf{r}} H_m(\bar{f}_x) H_n(\bar{f}_y), \quad (A2)$$

with the factor $(-i)^{m+n}$ added for technical convenience and the normalized Hermite polynomials being defined as

$$H_n(x) = \frac{1}{\sqrt{2^n n!}} (-1)^n e^{x^2} \frac{d^n}{dx^n} e^{-x^2}. \quad (A3)$$

Invoking the orthogonality of the Hermite polynomials with respect to the measure $\exp(-\bar{\mathbf{f}}^2)$, we obtain for the density modes,

$$\rho_{mn}(\mathbf{k}) = \frac{1}{\sqrt{N}} i^{m+n} \sum_{j=1}^{N} e^{i\mathbf{k}\cdot\mathbf{r}_j} H_m(\bar{f}_{j,x}) H_n(\bar{f}_{j,y}). \quad (A4)$$

The transient (or equilibrium-averaged) time-correlation between such density modes can then be defined via

$$S_{mn;m'n'}(\mathbf{k}, t) = \left\langle \rho_{mn}^*(\mathbf{k}) e^{\Omega^\dagger t} \rho_{m'n'}(\mathbf{k}) \right\rangle, \quad (A5)$$

where the adjoint (or backward) evolution operator is given by

$$\Omega^\dagger = \Omega_T^\dagger + \Omega_R^\dagger = \sum_{i=1}^{N} \left(D\nabla_i + \zeta^{-1}(\mathbf{F}_i + \mathbf{f}_i)\right) \cdot \nabla_i$$

$$+ \sum_{i=1}^{N} \left(\left(D_f \frac{\partial}{\partial \mathbf{f}_i} - \tau_p^{-1} \mathbf{f}_i\right) \cdot \frac{\partial}{\partial \mathbf{f}_i}\right). \quad (A6)$$

We adopt the convention that the adjoint evolution operator works on everything to its right except for the probability distribution. Note that the lowest order term $S_{00;00}(\mathbf{k}, t) \equiv F(k, t)$ corresponds to the intermediate scattering function, which will serve as the main probe to study glassy dynamics of our active system. At time zero, assuming our system to be isotropic, the density correlation functions are easily calculated and yield

$$S_{mn;m'n'}(k) = \left\langle \rho_{mn}^*(\mathbf{k})\rho_{m'n'}(\mathbf{k}) \right\rangle$$

$$= \delta_{mm'}\delta_{nn'}[1 + \delta_{m0}\delta_{n0}(S(k) - 1)], \quad (A7)$$

where $S(k)$ denotes the equilibrium static structure factor.

To arrive at an equation of motion for the intermediate scattering function, we will employ a similar strategy as already introduced for ABPs in Ref. 16. Starting from the Mori–Zwanzig projector formalism,[62,63] we introduce a projector on density modes (using the shorthand notation $l \equiv \{m, n\}$, which will be done throughout),

$$\mathcal{P} = \sum_{l_1} \sum_{l_2} \rho_{l_1}(\mathbf{k}) \Big\rangle S^{-1}_{l_1; l_2}(k) \Big\langle \rho^*_{l_2}(\mathbf{k})$$

$$= \sum_{l_1} \rho_{l_1}(\mathbf{k}) \Big\rangle S^{-1}_{l_1; l_1}(k) \Big\langle \rho^*_{l_1}(\mathbf{k}), \tag{A8}$$

and its orthogonal counterpart $\mathcal{Q} = 1 - \mathcal{P}$. Note that the superscript -1 represents the inverse matrix of the respective quantity, i.e., $X^{-1}_{l;l'} \equiv [\mathbf{X}^{-1}]_{l;l'}$. Following standard procedure in MCT one can then derive that

$$\frac{\partial}{\partial t} S_{l;l'}(\mathbf{k}, t) + \sum_{l_1} \omega_{l;l_1}(\mathbf{k}) S^{-1}_{l_1;l_1}(k) S_{l_1;l'}(\mathbf{k}, t)$$

$$- \int_0^t dt' \sum_{l_1} K_{l;l_1}(\mathbf{k}, t - t') S^{-1}_{l_1;l_1}(k) S_{l_1;l'}(\mathbf{k}, t') = 0. \tag{A9}$$

In this equation, the collective diffusion tensor, which governs the short-time dynamics, is given by

$$\omega_{l;l'}(\mathbf{k}) = -\Big\langle \rho^*_l(\mathbf{k}) \Omega^\dagger \rho_{l'}(\mathbf{k}) \Big\rangle$$

$$= \Big[k^2 D \delta_{ll'} + \zeta^{-1} \sqrt{D_f \tau_p} S_{l;l}(k) \, \mathbf{k} \cdot (\boldsymbol{\delta}_{ll'-} - \boldsymbol{\delta}_{ll'+}) \Big]$$

$$+ \Big[(m + n) \tau_p^{-1} \delta_{ll'} \Big]$$

$$\equiv \omega^{\mathrm{T}}_{l;l'}(\mathbf{k}) + \omega^{\mathrm{R}}_{l;l'}, \tag{A10}$$

where, we have introduced the two-vector $([\cdot, \cdot])$ shorthand notation,

$$\boldsymbol{\delta}_{ll'\pm} = \left[\sqrt{m' + \frac{1}{2} \pm \frac{1}{2}} \, \delta_{m,m'\pm 1} \delta_{nn'}, \sqrt{n' + \frac{1}{2} \pm \frac{1}{2}} \, \delta_{n,n'\pm 1} \delta_{mm'} \right]. \tag{A11}$$

The memory kernel, which represents all nontrivial dynamics, can be formally written as

$$K_{l;l'}(\mathbf{k}, t) = \Big\langle \rho^*_l(\mathbf{k}) \Omega^\dagger \mathcal{Q} e^{\mathcal{Q} \Omega^\dagger \mathcal{Q} t} \mathcal{Q} \Omega^\dagger \rho_{l'}(\mathbf{k}) \Big\rangle$$

$$= \Big\langle \rho^*_l(\mathbf{k}) \Omega^\dagger_{\mathrm{T}} \mathcal{Q} e^{\mathcal{Q} \Omega^\dagger \mathcal{Q} t} \mathcal{Q} \Omega^\dagger_{\mathrm{T}} \rho_{l'}(\mathbf{k}) \Big\rangle. \tag{A12}$$

Here, we have used that, since active degrees of freedom (self-propulsion forces) never slow down, the $\Omega^\dagger_{\mathrm{R}}$-terms do not contribute to the vertices, i.e., $\mathcal{Q} \Omega^\dagger_{\mathrm{R}} \rho_l(\mathbf{k})\rangle = \langle \rho_l(\mathbf{k}) \Omega^\dagger_{\mathrm{R}} \mathcal{Q} = 0$. Consequently, only the translational degrees of freedom yield slow dynamics and we, therefore, seek to convert the memory kernel to an irreducible (friction) memory kernel by means of the operators,

$$\mathcal{P}' = -\sum_{l_1 l_2} \rho_{l_1}(\mathbf{k}) \Big[\omega^{\mathrm{T}}_{l_1;l_2}(k) \Big]^{-1} \Big\langle \rho^*_{l_2}(\mathbf{k}) \Omega^\dagger_{\mathrm{T}}, \tag{A13}$$

and $\mathcal{Q}' = 1 - \mathcal{P}'$. Invoking Dyson decomposition, we may write

$$K_{l;l'}(\mathbf{k}, t) = M_{l;l'}(\mathbf{k}, t) - \int_0^t dt' \sum_{l_1 l_2} M_{l;l_1}(\mathbf{k}, t - t')$$

$$\times \Big[\omega^{\mathrm{T}}_{l_1;l_2}(\mathbf{k}) \Big]^{-1} K_{l_2;l'}(\mathbf{k}, t'), \tag{A14}$$

with the irreducible memory kernel defined as

$$M_{l;l'}(\mathbf{k}, t) = \Big\langle \rho^*_l(\mathbf{k}) \Omega^\dagger_{\mathrm{T}} \mathcal{Q} e^{\mathcal{Q} \Omega^\dagger \mathcal{Q}' \mathcal{Q} t} \mathcal{Q} \Omega^\dagger_{\mathrm{T}} \rho_{l'}(\mathbf{k}) \Big\rangle. \tag{A15}$$

Now, we can combine Eqs. (A9) and (A14) to arrive at an equation of motion for the intermediate scattering function, which lends itself to mode-coupling-like approximations,

$$\frac{\partial}{\partial t} S_{l;l'}(\mathbf{k}, t) + \sum_{l_1} \omega_{l;l_1}(\mathbf{k}) S^{-1}_{l_1;l_1}(k) S_{l_1;l'}(\mathbf{k}, t)$$

$$+ \int_0^t dt' \sum_{l_1 l_2} M_{l;l_1}(\mathbf{k}, t - t') \Big[\omega^{\mathrm{T}}_{l_1;l_2}(\mathbf{k}) \Big]^{-1}$$

$$\times \left[\frac{\partial}{\partial t'} S_{l_2;l'}(\mathbf{k}, t') + \omega^{\mathrm{R}}_{l_2;l_2} S_{l_2;l'}(\mathbf{k}, t') \right] = 0. \tag{A16}$$

We mention that this equation is identical in structure to the one obtained for ABPs in Ref. 16 and reiterate that, in comparison to the more familiar passive MCT equation, there is an additional hopping term $\omega^{\mathrm{R}}_{l_2;l_2} S_{l_2;l'}(\mathbf{k}, t')$ inside the time integral. This term ensures the long-time decay of the active degrees of freedom. At the same time, we also emphasize that the individual terms in the equation are not necessarily the same as the ones presented in Ref. 16 for ABPs, and these terms will, therefore, harbor the differences between the AOUP and ABP model.

To proceed and find a solution for the active-MCT equation, we project the fluctuating forces $\mathcal{Q} \Omega^\dagger_{\mathrm{T}} \rho_{l'}(\mathbf{k})$ onto density doublets. Specifically, we introduce, assuming Gaussian factorization for higher order static correlations[64] and making use of the fact that $S^{-1}_{l_1;l_2}(q)$ is diagonal, the projection operator,

$$\mathcal{P}_2 = \frac{1}{2} \sum_{\mathbf{q}_1 \mathbf{q}_2} \sum_{l_1 l_2} \rho_{l_1}(\mathbf{q}_1) \rho_{l_2}(\mathbf{q}_2) \Big\rangle S^{-1}_{l_1;l_1}(q_1) S^{-1}_{l_2;l_2}(q_2)$$

$$\times \Big\langle \rho^*_{l_1}(\mathbf{q}_1) \rho^*_{l_2}(\mathbf{q}_2), \tag{A17}$$

and use it to approximate

$$M_{l;l'}(\mathbf{k}, t) \approx \Big\langle \rho^*_l(\mathbf{k}) \Omega^\dagger_{\mathrm{T}} \mathcal{Q} \mathcal{P}_2 e^{\mathcal{Q} \Omega^\dagger \mathcal{Q}' t} \mathcal{P}_2 \mathcal{Q} \Omega^\dagger_{\mathrm{T}} \rho_{l'}(\mathbf{k}) \Big\rangle$$

$$= \sum_{\mathbf{q}_1 \cdots \mathbf{q}_4} \sum_{l_1 \cdots l_4} \Big\langle \rho^*_l(\mathbf{k}) \Omega^\dagger_{\mathrm{T}} \mathcal{Q} \rho_{l_1}(\mathbf{q}_1) \rho_{l_2}(\mathbf{q}_2) \Big\rangle S^{-1}_{l_1;l_1}(q_1)$$

$$\times S^{-1}_{l_2;l_2}(q_2) \Big\langle \rho^*_{l_1}(\mathbf{q}_1) \rho^*_{l_2}(\mathbf{q}_2) e^{\mathcal{Q} \Omega^\dagger \mathcal{Q}' t} \rho_{l_3}(\mathbf{q}_3) \rho_{l_4}(\mathbf{q}_4) \Big\rangle$$

$$\times S^{-1}_{l_3;l_3}(q_3) S^{-1}_{l_4;l_4}(q_4) \Big\langle \rho^*_{l_3}(\mathbf{q}_3) \rho^*_{l_4}(\mathbf{q}_4) \mathcal{Q} \Omega^\dagger_{\mathrm{T}} \rho^*_{l'}(\mathbf{k}) \Big\rangle. \tag{A18}$$

To make this expression tractable, we explicitly calculate both vertices. For convenience, we split the translational evolution operator into a passive and active contribution, i.e., $\Omega^\dagger_{\mathrm{T}} = \Omega^\dagger_{\mathrm{eq}} + \delta \Omega^\dagger_{\mathrm{T}}$,

with $\delta\Omega_{\mathrm{T}}^{\dagger} = \sum_i^N \zeta^{-1}\mathbf{f}_i \cdot \nabla_i$. Moreover, invoking the following orthogonality relation for Hermite polynomials,

$$
\pi^{-1/2}\int_{\infty}^{\infty} dx\, H_m(x)H_n(x)H_s(x)e^{-x^2}
$$
$$
= \sqrt{m!\,n!\,s!}\left[\left(\frac{m+n-s}{2}\right)!\left(\frac{s+n-m}{2}\right)!\left(\frac{s+m-n}{2}\right)!\right]^{-1}, \tag{A19}
$$

when $m+n+s$ is even, $m+n \geq s$, $s+n \geq m$, and $s+m \geq n$, or zero otherwise, and the conventional convolution approximation,[65] allows us to define a generalized convolution approximation given by

$$
\langle \rho_l^*(\mathbf{k})\rho_{l_1}(\mathbf{q}_1)\rho_{l_2}(\mathbf{q}_2)\rangle \approx \frac{1}{\sqrt{N}}\delta_{\mathbf{k},\mathbf{q}_1+\mathbf{q}_2} b_{m,m_1,m_2}
$$
$$
\times b_{n,n_1,n_2} S_{ll}(q)S_{l_1 l_1}(q_1)S_{l_2 l_2}(q_2). \tag{A20}
$$

Here, we have introduced the geometric factor,

$$
b_{n,n_1,n_2} = (-1)^{-(n-n_1-n_2)/2}\sqrt{n_1!\,n_2!\,n!}
$$
$$
\times \left[\left(\frac{n_1+n_2-n}{2}\right)!\left(\frac{n+n_2-n_1}{2}\right)!\left(\frac{n+n_1-n_2}{2}\right)!\right]^{-1}, \tag{A21}
$$

when $m+n+s$ is even, $m+n \geq s$, $s+n \geq m$, and $s+m \geq n$, or zero otherwise. Using the generalized convolution approximation, we have for the passive contribution of the left vertex,

$$
\langle \rho_l^*(\mathbf{k})\Omega_{\mathrm{eq}}^{\dagger}\mathcal{Q}\rho_{l_1}(\mathbf{q}_1)\rho_{l_2}(\mathbf{q}_2)\rangle S_{l_1;l_1}^{-1}(q_1)S_{l_2;l_2}^{-1}(q_2)
$$
$$
= \frac{\rho D}{\sqrt{N}}\delta_{\mathbf{k},\mathbf{q}_1+\mathbf{q}_2}(\mathbf{k}\cdot\mathbf{q}_1\,\delta_{l_1 0}\delta_{ll_2}c(q_1) + \mathbf{k}\cdot\mathbf{q}_2\,\delta_{l_2 0}\delta_{ll_1}c(q_2)), \tag{A22}
$$

where $c(q) = \rho^{-1}[1 - S^{-1}(k)]$ depicts the direct correlation function. Note that the passive contribution is thus a straightforward generalization of the standard MCT vertex. Furthermore, the passive contribution to the right vertex can be shown to take on an identical form.

For the active contribution to the left vertex, i.e.,

$$
\langle \rho_l^*(\mathbf{k})\delta\Omega_{\mathrm{T}}^{\dagger}\mathcal{Q}\rho_{l_1}(\mathbf{q}_1)\rho_{l_2}(\mathbf{q}_2)\rangle S_{l_1;l_1}^{-1}(q_1)S_{l_2;l_2}^{-1}(q_2), \tag{A23}
$$

we recall that $\mathcal{Q} = \mathcal{I} - \mathcal{P}$ and first consider the term,

$$
-\langle \rho_l^*(\mathbf{k})\delta\Omega_{\mathrm{T}}^{\dagger}\mathcal{P}\rho_{l_1}(\mathbf{q}_1)\rho_{l_2}(\mathbf{q}_2)\rangle S_{l_1;l_1}^{-1}(q_1)S_{l_2;l_2}^{-1}(q_2). \tag{A24}
$$

Using the generalized convolution approximation and Eq. (A10), this term can be written as

$$
-\frac{\zeta^{-1}}{\sqrt{N}}\sqrt{D_f \tau_p}\,\delta_{\mathbf{k},\mathbf{q}_1+\mathbf{q}_2} S_{l;l}(k)\,\mathbf{k}\cdot(\mathbf{b}_{l-l_1 l_2} - \mathbf{b}_{l+l_1 l_2}), \tag{A25}
$$

where, we have introduced

$$
\boldsymbol{b}_{ll_1^{\pm}l_2} = \left[\sqrt{m_1+\frac{1}{2}\pm\frac{1}{2}}\,b_{m,m_1\pm1,m_2}b_{n,n_1,n_2},\right.
$$
$$
\left.\sqrt{n_1+\frac{1}{2}\pm\frac{1}{2}}\,b_{m,m_1,m_2}b_{n,n_1\pm1,n_2}\right]. \tag{A26}
$$

Next, we also require an expression for

$$
\langle \rho_l^*(\mathbf{k})\delta\Omega_{\mathrm{T}}^{\dagger}\rho_{l_1}(\mathbf{q}_1)\rho_{l_2}(\mathbf{q}_2)\rangle S_{l_1;l_1}^{-1}(q_1)S_{l_2;l_2}^{-1}(q_2). \tag{A27}
$$

Exploiting the relation $2xH_n(x) = \sqrt{2(n+1)}H_{n+1}(x) + \sqrt{2n}H_{n-1}(x)$ and using the generalized convolution approximation, the above term can be calculated to give

$$
-\frac{\zeta^{-1}}{\sqrt{N}}\sqrt{D_f\tau_p}S_{l;l}(k)\delta_{\mathbf{k},\mathbf{q}_1+\mathbf{q}_2}\left[\mathbf{q}_1\cdot\left(\mathbf{S}_{ll_1^- l_2}(q_1) - \mathbf{b}_{ll_1^+ l_2}\right)\right.
$$
$$
\left.\times S_{l_1;l_1}^{-1}(q_1) + \mathbf{q}_2\cdot\left(\mathbf{S}_{ll_2^- l_1}(q_2) - \mathbf{b}_{ll_2^+ l_1}\right)S_{l_2;l_2}^{-1}(q_2)\right], \tag{A28}
$$

and is written in terms of

$$
\boldsymbol{S}_{ll_1^{\pm}l_2}(q) = \left[\sqrt{m_1+\frac{1}{2}\pm\frac{1}{2}}\,b_{m,m_1\pm1,m_2}b_{n,n_1,n_2}\right.
$$
$$
\times S_{m_1\pm1 n_1;m_1\pm1 n_1}(q),\ \sqrt{n_1+\frac{1}{2}\pm\frac{1}{2}}
$$
$$
\left.\times b_{n,n_1\pm1,n_2}b_{m,m_1,m_2}S_{m_1 n_1\pm1;m_1 n_1\pm1}(q)\right]. \tag{A29}
$$

The only term left to calculate is the active contribution to the right vertex. However, this term can be shown to yield a value of zero and, thus, does not contribute to the vertices. Combining all results, we then have for the memory kernel,

$$
M_{l;l'}(\mathbf{k},t) \approx \frac{\rho^2}{4N}\sum_{\mathbf{q}\mathbf{q}'}\sum_{l_1\ldots l_4} V_{ll_1 l_2}(\mathbf{k},\mathbf{q},\mathbf{k}-\mathbf{q})
$$
$$
\times \langle \rho_{l_1}^*(\mathbf{q})\rho_{l_2}^*(\mathbf{k}-\mathbf{q})e^{\mathcal{Q}\Omega^{\dagger}\mathcal{Q}'\mathcal{Q}t}\rho_{l_3}(\mathbf{q}')\rho_{l_4}(\mathbf{k}-\mathbf{q}')\rangle
$$
$$
\times V_{l'l_3 l_4}^{\mathrm{eq}}(\mathbf{k},\mathbf{q}',\mathbf{k}-\mathbf{q}'), \tag{A30}
$$

with the vertices given by

$$
V_{ll_1 l_2}^{\mathrm{eq}}(\mathbf{k},\mathbf{q},\mathbf{k}-\mathbf{q}) = D[\mathbf{k}\cdot\mathbf{q}\,\delta_{l_1 0}\delta_{ll_2}\,c(q)
$$
$$
+ \mathbf{k}\cdot(\mathbf{k}-\mathbf{q})\,\delta_{l_2 0}\delta_{ll_1}\,c(|\mathbf{k}-\mathbf{q}|)], \tag{A31}
$$

and

$$
V_{ll_1 l_2}(\mathbf{k},\mathbf{q},\mathbf{k}-\mathbf{q})
$$
$$
= V_{ll_1 l_2}^{\mathrm{eq}}(\mathbf{k},\mathbf{q},\mathbf{k}-\mathbf{q}) - \frac{\zeta^{-1}\sqrt{D_f\tau_p}}{\rho}S_{l;l}(k)
$$
$$
\times\left[\mathbf{k}\cdot(\mathbf{b}_{l-l_1 l_2} - \mathbf{b}_{l+l_1 l_2}) + \mathbf{q}\cdot(\mathbf{S}_{ll_1^- l_2}(q) - \mathbf{b}_{ll_1^+ l_2})S_{l_1;l_1}^{-1}(q)\right.
$$
$$
\left.+ (\mathbf{k}-\mathbf{q})\cdot(\mathbf{S}_{ll_2^- l_1}(|\mathbf{k}-\mathbf{q}|) - \mathbf{b}_{ll_2^+ l_1})S_{l_2;l_2}^{-1}(|\mathbf{k}-\mathbf{q}|)\right]. \tag{A32}
$$

To further simplify, the expression of the memory kernel, we employ the MCT-approximation and replace the four-point correlation function with projected dynamics by a product of two-point density correlation functions with full dynamics. This yields

$$\left\langle \rho_{l_1}^*(\mathbf{q})\rho_{l_2}^*(\mathbf{k}-\mathbf{q})e^{\mathcal{Q}\,\Omega^\dagger \mathcal{Q}'\mathcal{Q}t}\rho_{l_3}(\mathbf{q}')\rho_{l_4}(\mathbf{k}-\mathbf{q}') \right\rangle$$
$$\approx S_{l_1;l_3}(\mathbf{q},t)S_{l_2;l_4}(\mathbf{k}-\mathbf{q},t)\ \delta_{\mathbf{q},\mathbf{q}'} + S_{l_1;l_4}(\mathbf{q},t)S_{l_2;l_3}$$
$$\times (\mathbf{k}-\mathbf{q},t)\ \delta_{\mathbf{k}-\mathbf{q},\mathbf{q}'}. \tag{A33}$$

After taking the thermodynamic limit, one finally arrives at

$$M_{l;l'}(\mathbf{k},t) \approx \frac{\rho}{2} \int \frac{d\mathbf{q}}{(2\pi)^2} \sum_{l_1 l_2}\sum_{l_3 l_4} V_{ll_1 l_2}(\mathbf{k},\mathbf{q},\mathbf{k}-\mathbf{q})$$
$$\times S_{l_1;l_3}(\mathbf{q},t)S_{l_2;l_4}(\mathbf{k}-\mathbf{q},t)V_{l'l_3 l_4}^{\text{eq}}(\mathbf{k},\mathbf{q},\mathbf{k}-\mathbf{q}), \tag{A34}$$

which, using only the equilibrium static structure factor $S(k)$ as the initial boundary condition, allows us to self-consistently find a solution for $S_{l,l'}(\mathbf{k},t)$ and, in particular, for the intermediate scattering function $S_{00,00}(\mathbf{k},t) \equiv F(k,t)$. We conclude by mentioning that the above derivation can also be straightforwardly extended to three dimensions.

APPENDIX B: ROTATIONAL SYMMETRY

Due to the inclusion of the active degrees of freedom, dynamic correlation functions depend explicitly on the direction of the wavevector $\mathbf{k}$. However, we can bypass this problem by invoking the rotational symmetry of our system to align every wavevector entering correlation functions along a chosen direction. Suppose we rotate our coordinate axes clockwise over an angle θ (or all particles counter clockwise) such that

$$\mathbf{r}_j \to \mathbf{r}_j' = \mathbf{D}(\theta)\cdot\mathbf{r}_j, \quad \mathbf{f}_j \to \mathbf{f}_j' = \mathbf{D}(\theta)\cdot\mathbf{f}_j,$$

with the rotation matrix given by

$$\mathbf{D}(\theta) = \begin{pmatrix} \cos(\theta) & -\sin(\theta) \\ \sin(\theta) & \cos(\theta) \end{pmatrix}.$$

As a result, the AOUP density mode transforms like

$$\rho_{mn}(\mathbf{k}) \to \frac{1}{\sqrt{N}}i^{m+n}\sum_{j=1}^{N}e^{i\mathbf{k}'\cdot\mathbf{r}_j}H_m(\bar{f}_{j,x}')H_n(\bar{f}_{j,y}'),$$

where $\mathbf{k}' = \mathbf{D}^{\mathrm{T}}(\theta)\cdot\mathbf{k}$ depicts the rotated wavevector. Realizing that $\Omega^\dagger$, $P_{\text{eq}}(\Gamma_{\mathrm{T}})$, and $P(\Gamma_{\mathrm{R}})$ are invariant under such a rotation, and rewriting $H_l(\bar{f}_{j,x}')H_m(\bar{f}_{j,y}')$ back in terms of $\bar{\mathbf{f}}_j$ allows us to transform correlation functions with wavevector $\mathbf{k}$ to ones with wavevector $\mathbf{k}'$. Note that $\mathbf{k}$ is thus rotated clockwise. In the main text, we can, therefore, restrict our discussion to wavevectors aligned along a specific direction, which we have chosen to be the x-axis.

REFERENCES

[1] C. Bechinger, R. Di Leonardo, H. Löwen, C. Reichhardt, G. Volpe, and G. Volpe, Rev. Mod. Phys. **88**, 045006 (2016).
[2] S. Ramaswamy, Annu. Rev. Condens. Matter Phys. **1**, 323 (2010).
[3] M. C. Marchetti, J. F. Joanny, S. Ramaswamy, T. B. Liverpool, J. Prost, M. Rao, and R. A. Simha, Rev. Mod. Phys. **85**, 1143 (2013).
[4] L. M. C. Janssen, J. Phys.: Condens. Matter **31**, 503002 (2019).
[5] L. Berthier, E. Flenner, and G. Szamel, J. Chem. Phys. **150**, 200901 (2019).
[6] E. H. Zhou, X. Trepat, C. Y. Park, G. Lenormand, M. N. Oliver, S. M. Mijailovich, C. Hardin, D. A. Weitz, J. P. Butler, and J. J. Fredberg, Proc. Natl. Acad. Sci. U. S. A. **106**, 10632 (2009).
[7] B. R. Parry, I. V. Surovtsev, M. T. Cabeen, C. S. O'Hern, E. R. Dufresne, and C. Jacobs-Wagner, Cell **156**, 183 (2014).
[8] T. E. Angelini, E. Hannezo, X. Trepat, M. Marquez, J. J. Fredberg, and D. A. Weitz, Proc. Natl. Acad. Sci. U. S. A. **108**, 4714 (2011).
[9] K. Nishizawa, K. Fujiwara, M. Ikenaga, N. Nakajo, M. Yanagisawa, and D. Mizuno, Sci. Rep. **7**, 15143 (2017).
[10] S. Garcia, E. Hannezo, J. Elgeti, J.-F. Joanny, P. Silberzan, and N. S. Gov, Proc. Natl. Acad. Sci. U. S. A. **112**, 15314 (2015).
[11] S. Grosser, J. Lippoldt, L. Oswald, M. Merkel, D. M. Sussman, F. Renner, P. Gottheil, E. W. Morawetz, T. Fuhs, X. Xie, S. Pawlizak, A. W. Fritsch, B. Wolf, L.-C. Horn, S. Briest, B. Aktas, M. L. Manning, and J. A. Käs, Phys. Rev. X **11**, 011033 (2021).
[12] H. Lama, M. J. Yamamoto, Y. Furuta, T. Shimaya, and K. A. Takeuchi, "Emergence of bacterial glass: Two-step glass transition in 2D bacterial suspension," arXiv:2205.10436 (2022).
[13] N. Klongvessa, F. Ginot, C. Ybert, C. Cottin-Bizonne, and M. Leocmach, Phys. Rev. Lett. **123**, 248004 (2019).
[14] N. Klongvessa, F. Ginot, C. Ybert, C. Cottin-Bizonne, and M. Leocmach, Phys. Rev. E **100**, 062603 (2019).
[15] P. Arora, A. K. Sood, and R. Ganapathy, Phys. Rev. Lett. **128**, 178002 (2022).
[16] A. Liluashvili, J. Ónody, and T. Voigtmann, Phys. Rev. E **96**, 062608 (2017).
[17] G. Szamel, J. Chem. Phys. **150**, 124901 (2019).
[18] G. Szamel, E. Flenner, and L. Berthier, Phys. Rev. E **91**, 062304 (2015).
[19] G. Szamel, Phys. Rev. E **93**, 012603 (2016).
[20] M. Feng and Z. Hou, Soft Matter **13**, 4464 (2017).
[21] L. Berthier, Phys. Rev. Lett. **112**, 220602 (2014).
[22] R. Ni, M. A. C. Stuart, and M. Dijkstra, Nat. Commun. **4**, 2704 (2013).
[23] L. Berthier, E. Flenner, and G. Szamel, New J. Phys. **19**, 125006 (2017).
[24] L. Berthier and J. Kurchan, Nat. Phys. **9**, 310 (2013).
[25] E. Flenner and G. Szamel, Phys. Rev. E **102**, 022607 (2020).
[26] E. Flenner, G. Szamel, and L. Berthier, Soft Matter **12**, 7136 (2016).
[27] S. Henkes, Y. Fily, and M. C. Marchetti, Phys. Rev. E **84**, 040301 (2011).
[28] J. Reichert, S. Mandal, and T. Voigtmann, Phys. Rev. E **104**, 044608 (2021).
[29] J. Reichert and T. Voigtmann, Soft Matter **17**, 10492 (2021).
[30] J. Reichert, L. F. Granz, and T. Voigtmann, Eur. Phys. J. E **44**, 27 (2021).
[31] S. K. Nandi, R. Mandal, P. J. Bhuyan, C. Dasgupta, M. Rao, and N. S. Gov, Proc. Natl. Acad. Sci. U. S. A. **115**, 7688 (2018).
[32] R. Mandal and P. Sollich, Phys. Rev. Lett. **125**, 218001 (2020).
[33] G. Janzen and L. M. C. Janssen, Phys. Rev. Res. **4**, L012038 (2022).
[34] L. M. C. Janssen, A. Kaiser, and H. Löwen, Sci. Rep. **7**, 5667 (2017).
[35] D. Bi, X. Yang, M. C. Marchetti, and M. L. Manning, Phys. Rev. X **6**, 021011 (2016).
[36] V. E. Debets, X. M. de Wit, and L. M. C. Janssen, Phys. Rev. Lett. **127**, 278002 (2021).
[37] M. Paoluzzi, D. Levis, and I. Pagonabarraga, Commun. Phys. **5**, 111 (2022).
[38] Y.-E. Keta, R. L. Jack, and L. Berthier, Phys. Rev. Lett. **129**, 048002 (2022).
[39] T. F. F. Farage, P. Krinninger, and J. M. Brader, Phys. Rev. E **91**, 042310 (2015).
[40] S. K. Nandi and N. S. Gov, Soft Matter **13**, 7609 (2017).
[41] S. Ciarella, C. Luo, V. E. Debets, and L. M. C. Janssen, Eur. Phys. J. E **44**, 91 (2021).
[42] E. Flenner and G. Szamel, Phys. Rev. E **72**, 031508 (2005).

[43] M. Nauroth and W. Kob, Phys. Rev. E **55**, 657 (1997).

[44] F. Sciortino and W. Kob, Phys. Rev. Lett. **86**, 648 (2001).

[45] V. E. Debets, C. Luo, S. Ciarella, and L. M. C. Janssen, Phys. Rev. E **104**, 065302 (2021).

[46] G. Szamel and E. Flenner, Europhys. Lett. **133**, 60002 (2021).

[47] M. Fuchs and M. E. Cates, J. Rheol. **53**, 957 (2009).

[48] L. M. C. Janssen, Front. Phys. **6**, 97 (2018).

[49] W. Götze, *Complex Dynamics of Glass-Forming Liquids: A Mode-Coupling Theory* (Oxford University Press, Oxford, 2008).

[50] S. P. Das, Rev. Mod. Phys. **76**, 785 (2004).

[51] For a motivation of the specific form of the density modes we refer to the derivation in Appendix A and Ref. 16.

[52] G. Nägele, J. Bergenholtz, and J. K. G. Dhont, J. Chem. Phys. **110**, 7037 (1999).

[53] A. L. Thorneywork, S. K. Schnyder, D. G. A. L. Aarts, J. Horbach, R. Roth, and R. P. A. Dullens, Mol. Phys. **116**, 3245 (2018).

[54] F. Weysser, A. M. Puertas, M. Fuchs, and T. Voigtmann, Phys. Rev. E **82**, 011504 (2010).

[55] E. Lange, J. B. Caballero, A. M. Puertas, and M. Fuchs, J. Chem. Phys. **130**, 174903 (2009).

[56] Particle diameters are chosen such that the first four moments correspond to the results of a Gaussian distribution with a mean of 1 and a standard deviation of 0.1.

[57] S. Plimpton, J. Comput. Phys. **117**, 1 (1995).

[58] C. Kurzthaler, S. Leitmann, and T. Franosch, Sci. Rep. **6**, 36702 (2016).

[59] C. Kurzthaler, C. Devailly, J. Arlt, T. Franosch, W. C. K. Poon, V. A. Martinez, and A. T. Brown, Phys. Rev. Lett. **121**, 078001 (2018).

[60] E. Lång, A. Połeć, A. Lång, M. Valk, P. Blicher, A. D. Rowe, K. A. Tønseth, C. J. Jackson, T. P. Utheim, L. M. C. Janssen, J. Eriksson, and S. O. Bøe, Nat. Commun. **9**, 3665 (2018).

[61] H. Löwen, J. Chem. Phys. **152**, 040901 (2020).

[62] H. Mori, Prog. Theor. Phys. **33**, 423 (1965).

[63] R. Zwanzig, J. Chem. Phys. **33**, 1338 (1960).

[64] L. M. C. Janssen and D. R. Reichman, Phys. Rev. Lett. **115**, 205701 (2015).

[65] H. W. Jackson and E. Feenberg, Rev. Mod. Phys. **34**, 686 (1962).